Journal of Computational Physics 228 (2009) 2660–2675

Contents lists available at ScienceDirect

Journal of Computational Physics

journal homepage: www.elsevier.com/locate/jcp

Modeling merging and breakup in the moving mesh interface tracking method for multiphase flow simulations

Shaoping Quan [a,*], Jing Lou [a], David P. Schmidt [b]

[a] Large-Scale Complex Systems Programme, Institute of High Performance Computing, 1 Fusionopolis Way, #16-16 Connexis, Singapore 138632, Singapore
[b] Department of Mechanical and Industrial Engineering, The University of Massachusetts at Amherst, 160 Governors Dr., Amherst, MA 01003-2210, USA

ARTICLE INFO

Article history:
Received 10 June 2008
Received in revised form 13 November 2008
Accepted 22 December 2008
Available online 3 January 2009

Keywords:
Moving mesh interface tracking
Mesh adaptation
Mesh separation
Mesh combination
Tetrahedral mesh
Coalescence
Breakup
Multiphase flows

ABSTRACT

The three-dimensional, moving mesh interface tracking (MMIT) method coupled with local mesh adaptations by Quan and Schmidt [S.P. Quan, D.P. Schmidt, A moving mesh interface tracking method for 3D incompressible two-phase flows, J. Comput. Phys. 221 (2007) 761–780] demonstrated the capability to accurately simulate multiphase flows, to handle large deformation, and also to perform interface pinch-off for some specific cases. However, another challenge, i.e. how to handle interface merging (such as droplet coalescence) has not been addressed. In this paper, we present a mesh combination scheme for interface connection and a more general mesh separation algorithm for interface breakup. These two schemes are based on the conversion of liquid cells in one phase to another fluid by changing the fluid properties of the cells in the combination or separation region. After the conversion, the newly created interface is usually ragged, and a local projection method is employed to smooth the interface. Extra mesh adaptation criteria are introduced to handle colliding interfaces with almost zero curvatures as the distance between the interfaces diminishes. Simulations of droplet pair collisions including both head-on and off-center coalescences show that the mesh adaptations are capable of resolving very small length scales, and the mesh combination and mesh separation schemes can handle the topological transitions in multiphase flows. The potential of our method to perform detailed investigations of droplet coalescence and breakup is also displayed.

1. Introduction

In previous work [1], Quan and Schmidt presented a three-dimensional, moving mesh interface tracking (MMIT) method to simulate multiphase flows using an unstructured tetrahedral mesh with a finite volume method. The interface is of zero thickness and moves with the fluids, and thus the jump conditions across the interface are implemented directly without any smoothing. Local mesh adaptations including mesh coarsening and mesh refining are introduced for both the interior and the interface elements to maintain good mesh quality, to achieve enough mesh resolution, to capture the changing curvature, and to obtain computational efficiency. However, handling topological transitions, such as liquid particle (bubble or droplet) collision and pinch-off, is a challenge for this direct numerical method. Here, we propose a mesh combination method and a more general mesh separation scheme to simulate the coalescence and the breakup of liquid particles in multiphase flow systems using the MMIT method.

* Corresponding author. Tel.: +65 64191251; fax: +65 64674350.
E-mail address: quansp@ihpc.a-star.edu.sg (S.P. Quan).

0021-9991/$ - see front matter © 2008 Elsevier Inc. All rights reserved.
doi:10.1016/j.jcp.2008.12.029

Modeling of droplet (bubble) collision and breakup has been a subject of interest for decades, both experimentally and theoretically, and also numerically due to the fundamental importance of a variety of multiphase flow systems, such as sprays, liquid–liquid extractors, and ink-jet printing. There is a large body of literature on experimental and theoretical studies, such as the following examples [2–11].

Numerical methods for simulating multiphase flows, including modeling of topological changes, have significantly advanced over the last fifteen years. Older work by Lafaurie et al. [12] presented the SURFER program based on the volume of fluid (VOF) method and simulated droplet collision both in two and three-dimensions including interface breakup and reconnection. The method conserves mass exactly, however, parasitic currents were reported. Recently, Gotaas et al. [13] investigated droplet–droplet collisions both experimentally and numerically. The effect of viscosity on the collision outcome was studied, and they pointed out that numerical simulations using VOF were "only for visual comparisons". Sussman et al. [14] developed a level set method to compute the motion of incompressible two-phase flows. In their method, merging and breaking of the interface were automatically taken care of as the level set function, which was employed to capture the interface, is a smooth function. They simulated two water droplets colliding with each other and a rising bubble with satellite droplets pinched off at the rear to show the capability of the method to deal with complex multiphase flow problems. More recently, using a level set method, Pan and Suga [15], and Tanguy and Berlemont [16] simulated binary droplet collisions, and their results agreed qualitatively with experimental observations by Qian and Law [6] and by Ashgriz and Poo [5], respectively. Inamuro et al. [17] developed a lattice Boltzmann method to model incompressible two-phase flows, and simulations of droplets colliding and bubbles coalescence were presented in their work.

Nobari et al. [18] performed two-dimensional axisymmetric simulations of head-on droplet collisions using a front-tracking finite difference method. Nobari and Tryggvason [19] also presented simulations of three-dimensional droplet collision. In their method, the merging of the interface was performed using an interface reconstruction method, in which the interface elements that are very close and nearly parallel were removed and the rest of the elements were reconstructed to form a single interface. A common criticism of the front tracking method is the complexity in handling the merging and breakup of the interfaces in three-dimension. To simplify the treatment of topological changes in three-dimensional multiphase flows, Torres and Brackbill [20] proposed a point-set method, which actually is a front tracking method without logical connectivity of the interfacial points. The interfacial points were regenerated periodically according to a smooth indicator function. By treating the interfacial points in such a way, the implementation of interface merging and breakup in three-dimension is much simpler. However, Shin and Juric [21] describe the point-set method as "cumbersome" and more computationally expensive than standard front tracking. They developed a level contour reconstruction scheme for the front tracking method, in which the logical connectivity of interfacial points was not maintained. They pointed out that their technique made the modeling of the merging and breakup of the interfaces in three-dimension automatic. Three-dimensional simulations of bubbles merging, and droplets collision and breakup were presented in their work.

Sharp interface methods such as the immersed interface method [22,23] and the Ghost fluid method [24,25] have also been developed. Recently, Sussman et al. [26] proposed a sharp interface method for incompressible two-phase flows based on the coupling of level-set and volume-of-fluid. They pointed out that for the problems with high Reynolds number, the method is second order accurate, while the method is first order for the flows where viscous forces are dominant. Nourgaliev et al. [27] presented a sharp interface method for a fluid–fluid interface, and they showed that the sharp interface method satisfies the jump conditions across the interface within one cell.

The MMIT method used in the present work also falls in the category of sharp interface methods. The salient features of the MMIT method are, (1) the interface is zero-thickness; (2) the interface elements are cell faces; (3) thus, the jump conditions across the interface are implemented directly on the zero-thickness interface. The MMIT method is especially convenient for the discontinuity in the densities of the two-fluids, since the Lagrangian motion of interface elements prohibits any numerical mixing.

It can be seen that topological transitions in most of the above-mentioned methods are usually handled indirectly. However, detailed studies of the physics of initial coalescence, such as the gap width history of near-contact motion of droplet pairs and the history of the radius of the bridge which connects two droplets to initiate the coalescence, are lacking and remain a challenge for these methods. Using a boundary integral method coupled with adaptive restructuring meshes on evolving surfaces, Cristini et al. [28] simulated droplet breakup and also near-contact motion of a pair of deformable drops. Gap width histories of the droplet pair coalescence were shown in their work. A mesh splicing scheme was employed in their method for handling of the breakup of the interface. Recently, Anderson et al. [29] generalized the adaptive surface remeshing algorithm by Cristini et al. [28] to volume domains, and Zheng et al. [30] applied this generalized remeshing scheme coupled with a finite-element/level-set method to simulate 3D droplet breakup.

Dai and Schmidt [31] used a moving mesh method to simulate three-dimensional head-on collisions of two equal-sized droplets. However, in their work free-surface flows were considered by assuming a vacuum environment, and the two droplets were initially connected. The aim of this paper is to propose a mesh combination method and a more general mesh separation scheme for MMIT to directly simulate the challenging problems in multiphase flows, such as droplets coalescence and breakup in another viscous fluid. The capability of the method to perform detailed investigations of these problems is also presented. The paper is organized as follows. In Section 2, a brief review of the governing equations and the numerical method is given. In Section 3, mesh adaptation methods are reviewed and extra mesh adaptation criteria are introduced. Mesh combination and mesh separation are presented in Section 4. Three-dimensional droplet coalescence, including head-on and off-center collision, are displayed in Section 5. Concluding marks and discussions are given in Section 6.

2. Governing equations and numerical method

In this section, only a review of the governing equations and the numerical methods for solving the governing equations are given; the details and validations of the method can be found in [1,32–34]. The integral form of the Navier–Stokes equations in a moving and deforming control volume for incompressible, immiscible multiphase flow systems can be expressed as

$$\frac{d}{dt}\int\int\int_{CV} dv = \int\int_{CS} \mathbf{v}\cdot\mathbf{n}\,ds, \tag{1}$$

$$\frac{d}{dt}\int\int\int_{CV} \rho dv + \int\int_{CS} \rho(\mathbf{u}-\mathbf{v})\cdot\mathbf{n}\,ds = 0, \tag{2}$$

$$\frac{d}{dt}\int\int\int_{CV} \rho\mathbf{u} dv + \int\int_{CS} \rho\mathbf{u}(\mathbf{u}-\mathbf{v})\cdot\mathbf{n}\mathbf{d}\mathbf{s} = \int\int\int_{CV} \rho\mathbf{f} dv - \int\int_{CS} p\mathbf{n}\,ds + \int\int_{CS} \mu(\nabla\mathbf{u}+\nabla\mathbf{u}^T)\cdot\mathbf{n}\,ds, \tag{3}$$

where *CV* and *CS* denote a control volume and the surfaces of the control volume, **u**, **v**, **n**, and **f** stand for the fluid velocity, the velocity of a moving control volume, the unit normal vector of the face, and the body force per unit mass, respectively, and the superscript *T* is the transpose. Eq. (1) is a relationship between the rate of change of volume and the surface integral of the moving mesh velocity of a control volume. The jump in the fluids' density across the interface presents no difficulties because the convection terms in Eqs. (2) and (3) are identically zero on the interface for the moving mesh interface tracking method where the interface evolves with the fluids, i.e. $\mathbf{v}=\mathbf{u}$.

The viscous shear stresses on the interface are computed by a geometric harmonic mean method [1,35]. The interfacial curvatures are calculated using a least-squares parabola fitting in a local coordinate system, and the surface tension forces are implemented as a pressure boundary condition on the interface. The jumps in normal viscous stresses are implemented directly by using a Taylor series expansion. The governing equations are solved in a discrete stream function formulation, and the three-dimensional stream function vectors are defined at the edge centers. An exact fractional step method [36] is employed to avoid solving a pressure Poisson equation. The Crank–Nicolson scheme is used for viscous terms, and a central difference scheme is applied for the convection terms. A three-step, second order, Runge–Kutta scheme is employed for time integration [34]. The time step is limited by three stability criteria, namely, CFL, surface tension due to the explicit scheme, and mesh Peclet number [1]. Therefore, for the simulations, small cells require small time-steps. The resulting linear equation system is solved by a diagonal preconditioned Conjugate Gradient scheme. The preconditioner is proportional to the inverse of the cell volume, which is used to ease the stiffness of the matrix due to large difference in cell volume as a result of the local mesh adaptations.

3. Mesh adaptations

In the MMIT method, the interface mesh nodes evolve with the flow while the interior nodes are relocated in an optimization-based smoothing fashion [33]. Mesh adaptations including edge swapping, edge bisection, and edge contraction [33,1] are applied locally to achieve good mesh quality as well as to avoid global remeshing. For each adaptation, interpolation of the velocity field is needed because new elements are usually created or there are some geometrical changes in the old cells. However, the errors due to the interpolation are believed to be very small because in a typical time step, less than 0.3% of the elements undergo topological changes, requiring the interpolation.

The criterion for the interface edge bisection and contraction used in our previous work is the local curvature. However, this criterion is not sufficient for two nearly flat interfaces approaching each other with the distance between the two interfaces much smaller than the local interface radius. This configuration could appear when two deformable liquid particles approach each other with a gap (drainage) between them. In order to address this problem, a local averaged length scale of the interior edges is introduced. For an interface edge, the local averaged length scale (l_0) is the average of the length of the interior edges which connect to the two nodes of the interface edge, i.e.

$$l_0 = \alpha\frac{1}{N}\sum_{\text{Edges}} l_e, \tag{4}$$

where α is a constant and is used to adjust the mesh resolution (usually we choose a value in the range of 1.5–2.0), N is the number of the edges connected to the interface edge, and l_e is the length of the interior edge. Then, the criterion for the interface edges is the minimum of l_0 and the local radius. Cristini et al. [28] proposed a length scale for closely spaced surfaces, and the length scale is a function of the quadratic variation of the local gap width.

To further test the mesh adaptation schemes and the criterion based on the minimum of the averaged length of the interior edges and the local radius, near-contact motion of a pair of deformable droplets is simulated. The two droplets are initially spherical and move toward each other with uniform velocities. Fig. 1 shows the meshes for the case, where, for clarity, the droplets are colored red and the suspending phase colored blue. It should be noted that, although different colors are used to display the meshes, the meshes of the droplets and the suspending fluid are connected via the interface triangles to form a single mesh, and this single mesh is used for simulations. The gap width is as small as 1.5% of the diameter of

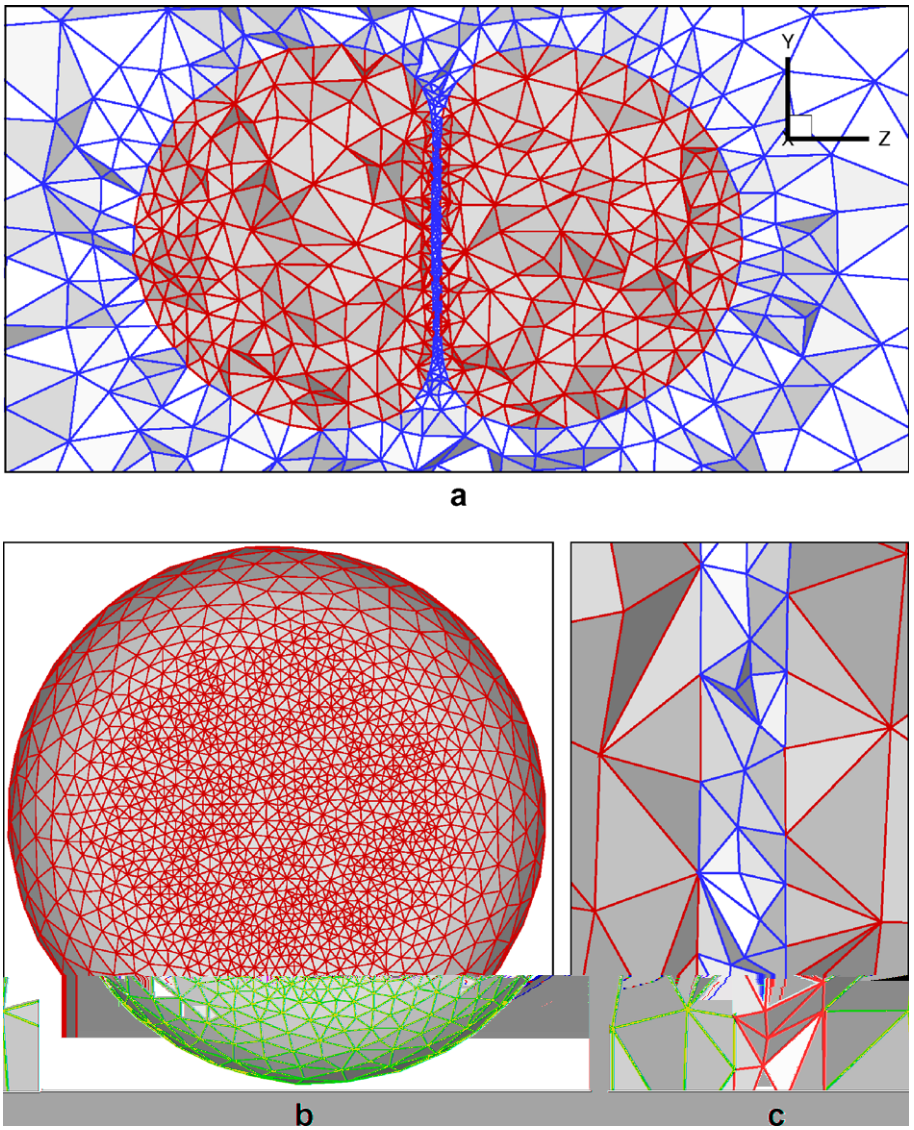

Fig. 1. Mesh adaptation for the interior and the interface for a case where two deformable droplets approach each other in another viscous fluid. (a) Meshes of the droplets (red and dark shade) and the suspending fluid (blue and light shade). (b) Surface mesh of one of the droplets, looking along the axis of collision. (c) Enlarged view of meshes near the gap in *yz* plane. (For interpretation of the references in colour in this figure legend, the reader is referred to the web version of this article.)

the initial droplet in the figure. Fig. 1(a) displays the interior meshes for the both phases in *yz* plane. The mesh near the droplets is much finer than that far away from the droplets, and the mesh near the gap is hardly perceivable. Detailed views of the interface mesh and the mesh near the gap region are shown in Fig. 1(b) and (c). It is clear that the interfacial mesh in the flattened region near the gap is fine enough to maintain good mesh quality and to achieve necessary resolution. The mesh away from the gap is coarse as the local radius is the criterion for the edge bisection.

4. Mesh combination and mesh separation

Droplet/bubble collision occurs frequently in many multiphase flow applications, such as dense sprays and air bubbles rising in water. Coalescence or pinching represents a topological change in the interface. These processes involve extremely small length scales. The MMIT scheme resolves the variable length scales whereas most of the fixed-mesh schemes automatically handle such topological changes. Thus the MMIT scheme offers faithful representation of small-scale phenomena, but requires additional computational effort and more complex heuristics. At some point, the further resolution of the interface singularities provides no additional benefit, at which point the interface merging or separation should proceed. Resolution *ad*

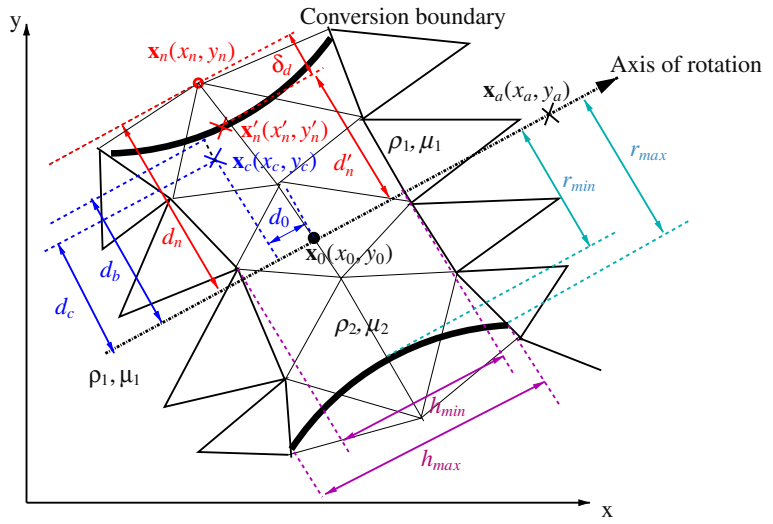

Fig. 2. Two-dimensional sketch of mesh combination. The phase 1 (droplets) with ρ_1 and μ_1 is denoted by thick triangles, and the suspending phase with ρ_2, μ_2 thin triangles. The two smooth, thick, solid curves are the curve of the projection. A thin film is in the suspending phase (ρ_2, μ_2).

infinitum would be expensive and pointless, since additional phenomena such as Van Der Waals forces would become dominant. In order to deal with the interface merging in the MMIT method, a mesh combination scheme is introduced.

A combination zone is located by the physics of the problem or by some numerical procedures. Here, the outer boundary (conversion boundary) of the connection region is assumed to be a curve in 2D (see Fig. 2) or a surface of revolution of a curve in 3D (see Fig. 3(a) for two nearly spherical droplets head-on collision). The axis of rotation (conversion axis) is also identified, and two points on the axis are also obtained with $\mathbf{x}_0$ as the center of the conversion region and $\mathbf{x}_a$ as an arbitrary point (which must be different from $\mathbf{x}_0$) on the axis. Our simulations are three-dimensional, and Fig. 2 is employed to more clearly present the algorithm of the combination scheme. The suspending phase is denoted by thin triangles and the droplets by thick triangles in Fig. 2, while in 3D the suspending phase is shaded green and droplet gray (see Fig. 3(a)).

The cells in the suspending phase and with the cells centers $(\mathbf{x}_c)$ located inside the conversion boundary are converted to droplet cells by changing the fluid properties (ρ and μ) of the cells to the droplet phase's. Here, to determine whether a cell is located inside the conversion boundary, the distance from the cell center to the axis is calculated by the formula of the three-dimensional point-line distance as

$$d_c = \frac{|(\mathbf{x_a} - \mathbf{x_0}) \times (\mathbf{x}_0 - \mathbf{x}_c)|}{|\mathbf{x}_a - \mathbf{x}_0|}, \tag{5}$$

where $\times$ stands for the cross product, and $|\cdot|$ denotes the vector L^2 norm. For 2D calculations, one could simply set all vectors with zero z-components. The distance (d_b) from the conversion boundary to the axis of rotation is only a function of the length (d_0) in the direction of the axis of rotation from the cell center to the center of the combination zone. For example, for the cell with centroid $\mathbf{x}_c, d_0$ is obtained by performing a dot-product of vectors as

$$d_0 = \frac{|(\mathbf{x_c} - \mathbf{x_0}) \cdot (\mathbf{x}_a - \mathbf{x}_0)|}{|\mathbf{x}_a - \mathbf{x}_0|}. \tag{6}$$

For the cells to be converted, $d_c \leqslant d_b$. It should be noted that in our current scheme, the curve of the conversion boundary is quadratic rather than linear in order to obtain a smooth connection between the combination region and the two droplets. For simplicity, the curve is also symmetric about the axis (or plane in 3D) perpendicular to the axis of rotation and through the center of the combination region.

After the conversion of the interior cells, the newly created interface might not be smooth. The image on the right of Fig. 3(a) shows the interior cells after the conversion, and it can be seen that the part of the original interface at the conversion region becomes interior faces and a new interface is created as well. The elements (faces, edges, nodes) on the new interface are converted to interface elements by changing their markers. The details of the newly created interface mesh are shown on the left hand of Fig. 3(b). It is clear that the new interface is so rough that the simulation can not be continued, as the calculated curvature in this region is erroneous. In order to make the new interface smooth, the vertices $(\mathbf{x}_n)$ on the new interface are moved to the conversion boundary utilizing a projection and a number of sub-steps with interior mesh adaptations to avoid any invalid cells. More specifically, for the newly created interface node $\mathbf{x}_n$, the deviation (δ_d) to the projected position $(\mathbf{x}'_n)$ is the difference between the distance (d_n) from $\mathbf{x}_n$ to the axis and the distance (d'_n) from the projection $(\mathbf{x}'_n)$ of this interfacial node to the curve, i.e. $\delta_d = d_n - d'_n$, where d_n can be obtained by Eq. (5), and d'_n is computed using

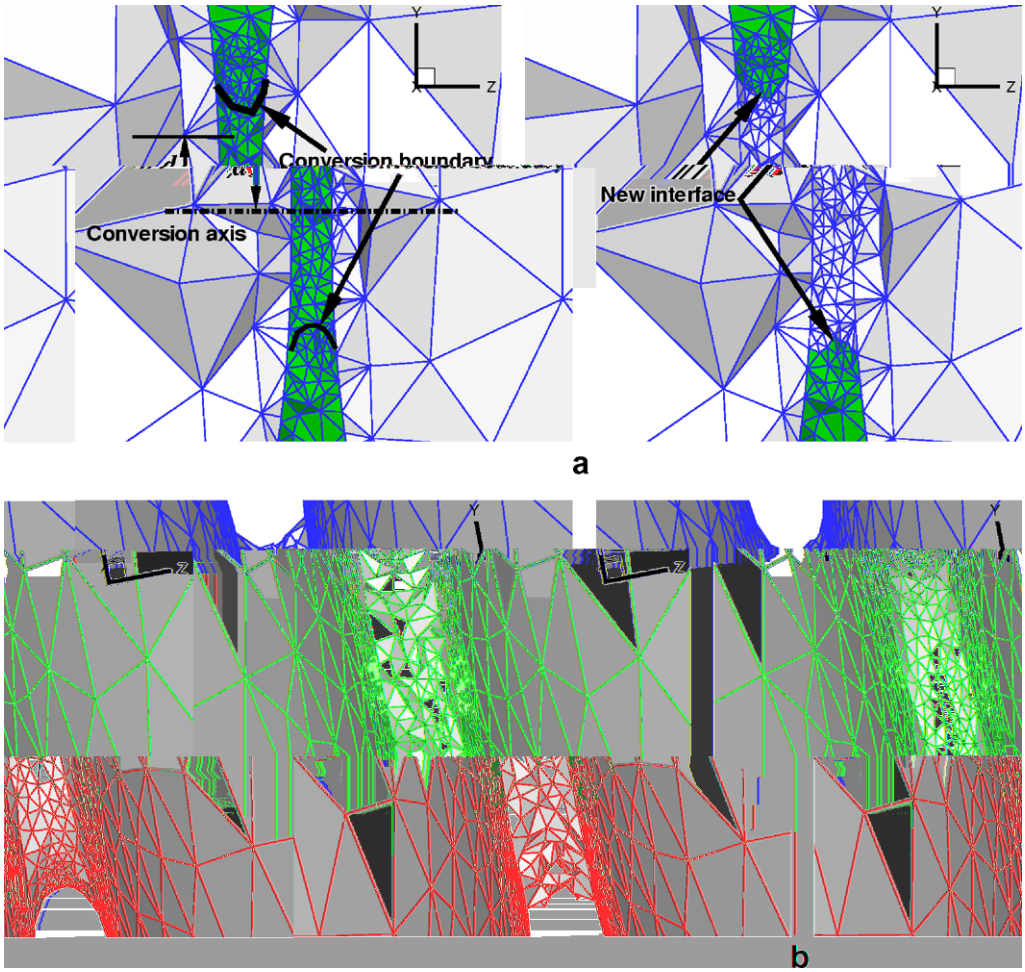

Fig. 3. Mesh combination. (a) Interior meshes before and after the combination. The droplet phase is shaded gray and the suspending fluid green). After the combination, a bridge connecting the two droplets is formed. (b) Surface meshes near the bridge of the droplets before and after projection. (For interpretation of the references in colour in this figure legend, the reader is referred to the web version of this article.)

the curve equation. However, it should be noted that if node $\mathbf{x}_n$ is moved to the projection position $\mathbf{x}'_n$ in one step, there might be mesh tangling and/or degenerated elements, which will eventually halt the simulation. In order to avoid invalid cells, the node is moved gradually to the position in a number of steps (currently, we move the node in 50 steps, i.e. for every step, the node is moved by $\frac{\delta_d}{50}$). At each step, mesh adaptations including edge swapping, optimization based interior mesh smoothing, and interfacial mesh smoothing [33,1] are applied to maintain good mesh quality. The interface after the projection is displayed in the view on the right side of Fig. 3(b), and it is clear the interface is smooth enough to continue the simulations. It should be noted that, although, the example shown here is a special case where the axis of rotation coincides with z-axis, the combination scheme is general, which will be demonstrated in the simulation of off-center droplets collision in the next sections.

It can be observed clearly that there is a small mass gain for the droplet phase and mass loss for the suspending fluid. However, the mass gain error (m_g) for the droplets based on the mass of the two initial spherical droplets satisfies,

$$3\left(\frac{r_{\min}}{D}\right)^2 \frac{h_{\min}}{D} \leqslant m_g \leqslant 3\left(\frac{r_{\max}}{D}\right)^2 \frac{h_{\max}}{D}, \tag{7}$$

where $r_{\min}$ and $r_{\max}$ are the smallest and largest radius of the surface of rotation, $h_{\min}$ and $h_{\max}$ denote the smallest gap width and the largest gap width (see Fig. 2), and D is the diameter of the initial sphere. Because the relative mass of the suspending phase is dependent on the size of computational domain, the mass gain error based on the droplets is given here. For the case shown in Fig. 3, where the smallest distance $(h_{\min})$ between two droplets is around 1.5% of the diameter of the droplet, and the smallest radius $(h_{\min})$ of the bridge is about 10%, the error of mass gain is as small as 0.045%. It is believed that the momentum error due to the conversion is also very tiny. It is clear that a smaller radius and/or smaller gap width would decrease the mass gain or loss as well as momentum error in exchange for greater computational cost.

To summarize the mesh combination scheme, the algorithm is given below.
Listing 1. Psuedo-code for combining separate droplet sub-meshes

```
set center and axis positions, x0 and xa
cellMarker(:) = NULL
do i = 1, number of cells
  if(cell(i) is in the suspending phase)
    calculate dc using Eq. (5)
    compute d0 by Eq. (6)
    compute db using the curve equation
    if (dc < db)
      cellMarker(i) = DROPLET
      convert the cell to droplet phase
    else
      cellMarker(i) = GAS
do i = 1, number of cells
  if (cellMarker(i) == DROPLET)
    do j = 1, number of cell faces
      if(two neighboring cells have different cellMarkers)
        label the new interfaces, the edges, and nodes
do i = 1, number of nodes
  if(node(i) is a new interfacial node)
    calculate dn using Eq. (5)
    compute d'n using Eq. (6) and the curve equation
    δd = dn − d'n
do i = 1, number of sub-steps
  move new interfacial nodes by the deviation (δd)/number of sub-steps
  proceede with mesh adaptations:
  edge swapping
  optimization-based interior mesh smoothing
  interfacial mesh smoothing
```

The mesh separation scheme in the prior publication [1] can only be applied to the cases where the pinch-off part has a cutting plane which aligns with one of the global axes (x-, y-, or z-axis), where distances can be easily calculated by subtracting the value of the axis. However, in most cases where the pinch-off occurs, the cutting plane does not align with any of the global axis. Here a general scheme is proposed that can handle any orientation as well as differing drop sizes. First, a cutting plane, the width (w_d) of the conversion region, and the center ($\mathbf{x}_0$) of the separation region are identified as shown in Fig. 4,

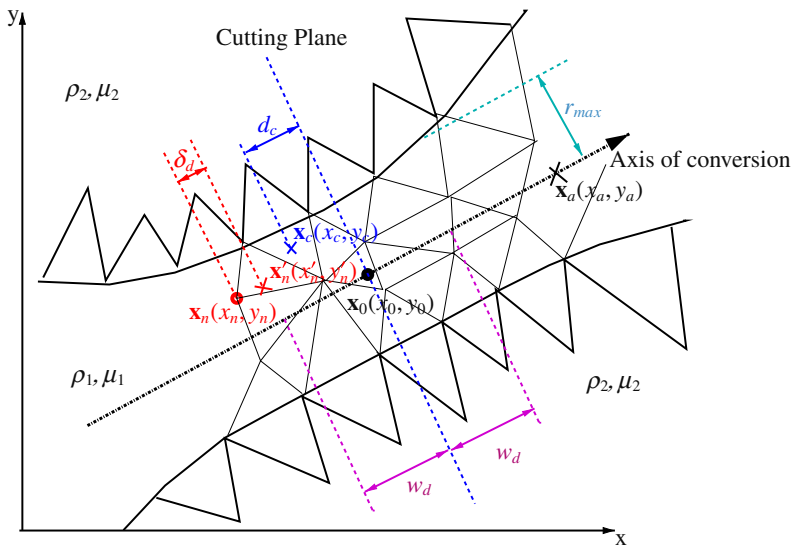

Fig. 4. Two-dimensional sketch of mesh separation. The droplet phase with ρ_1, μ_1 is denoted by thick triangles, and the suspending phase with ρ_2, μ_2 by thin triangles. A thin thread is in the droplet phase.

where only a 2D sketch is displayed. To calculate the shortest distance (d_c) from the cell center $(\mathbf{x}_c)$ to the cutting plane, the equation of the plane is needed. However, a more convenient way for computing the distance is specify a line through $\mathbf{x}_0$ and normal to the plane. Here, this line is denoted by $\mathbf{x}_0$ and $\mathbf{x}_a$, and is referred as the axis of conversion. This axis of conversion is usually the axis of symmetry of the thin liquid thread. Then, the smallest distance (d_c) from the cell center in the liquid particle phase to the cutting plane is calculated by performing a dot-product of the vector from the cell center to the center of the separation and the unit vector of the axis of conversion by utilizing Eq. (6). If the distance (d_c) is less than the width (w_d) of the separation region, the cell is converted to the suspending phase by changing the fluid properties. Then, the projection method similar to the one in [1] is applied to the newly created interfaces to make them smooth. The deviation (δ_d) for the new interface node to move to the projection position is also calculated based on the dot-product (Eq. (6)) rather than simply performing the subtraction as in previous work [1]. It should be also noted that the center of the local spheres for the two newly created interfaces might not be exactly on the axis of the conversion. The average of the node position of the newly interfacial nodes for each side is used as the center for each local sphere. The mass loss (M_l) can be estimated as

$$M_l \leqslant 2\rho_1 \pi r_{\max}^2 w_d. \tag{8}$$

The lower bound of the net mass loss is potentially extremely small due to the projection method which moves the new interfacial nodes outward and in turn gains mass for the droplet phase.

5. Numerical results

In this section, a number of numerical simulations of colliding droplets including head-on and off-center are performed to test the capability of the mesh adaptation, mesh separation, and mesh combination. The outer domain is a box with a length of $16D$, a width of $12D$, and a height of $12D$, where D is the diameter of the spherical droplet. The droplets are located in the center. No-slip boundary conditions are applied to the outer walls. The density ratio $(\eta = \rho_d/\rho_s)$ and viscosity ratio $(\lambda = \mu_d/\mu_s)$ are 10.0 for all the simulations, where the subscript d stands for the droplet phase, and s the suspending fluid.

5.1. Near-contact motion of head-on collision

Two droplets' approach towards each other with *an initial speed* (U_c) of the centroid of each droplet in an otherwise quiescent fluid is simulated, and the Reynolds number based on the droplet properties $\left(Re = \frac{\rho_d(2U_c)D}{\mu_d}\right)$ is 20.0. The Weber number based on the droplet properties $\left(We = \frac{\rho_d(2U_c)^2 D}{\sigma}\right)$ is 8.0, where D is the diameter of the initial spherical droplet, and σ denotes the surface tension coefficient and is assumed a constant. Because stream functions are the basic unknowns in our finite volume method, in order to initialize the droplets with uniform velocities and the suspending phase with zero velocities, a linear stream function is applied to the edges in the droplet phase with a zero value for the edge with the center located at z-axis, while the stream function in the suspending phase is set to zero. However, care must be taken to construct a divergence free and smooth initial condition for this droplet collision system, as large momentum errors are created near the interface due to the discontinuities in the stream functions and fluid velocities across the interface, as shown in Fig. 5(a). Obviously, a reasonable result cannot be obtained with this initial velocity field. To overcome this problem, the simulation is run with no mesh motion and by treating the droplets as solids for some time. The velocity errors near the interface will be smoothed out, and thus a continuous velocity field is obtained, which is displayed in Fig. 5(b). This smoothed velocity field is used as the initial condition for the simulation.

Fig. 6 shows the evolution of two deformable droplets colliding head-on, where time is non-dimensionalized by $t_c = D/U_c$. As time progresses, the portions of the droplets close to each other become flattened. The smallest distance between the two droplets are increasingly small, and finally a thin film drainage is created between the two droplets. Though the two interfaces in the gap region seems almost parallel in Fig. 6(d), a detailed view of the gap region in Fig. 7 shows that the gap film interfaces are not parallel. Fig. 7 shows an xz cut of the two droplets through the droplets' centers, and it can be

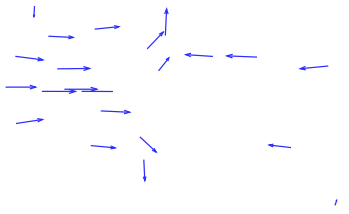

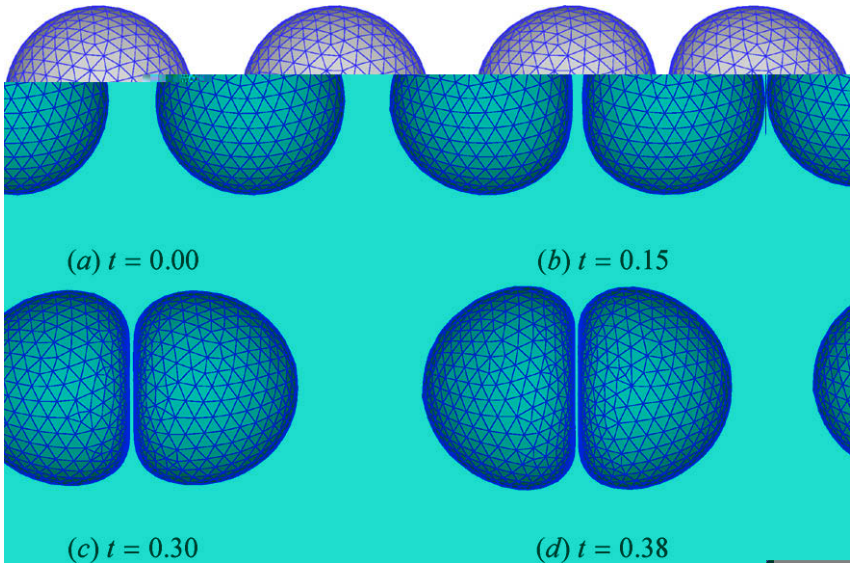

Fig. 6. Evolution of droplets' shapes. $Re = 20.0$ and $We = 8.0$. Time t is non-dimensional.

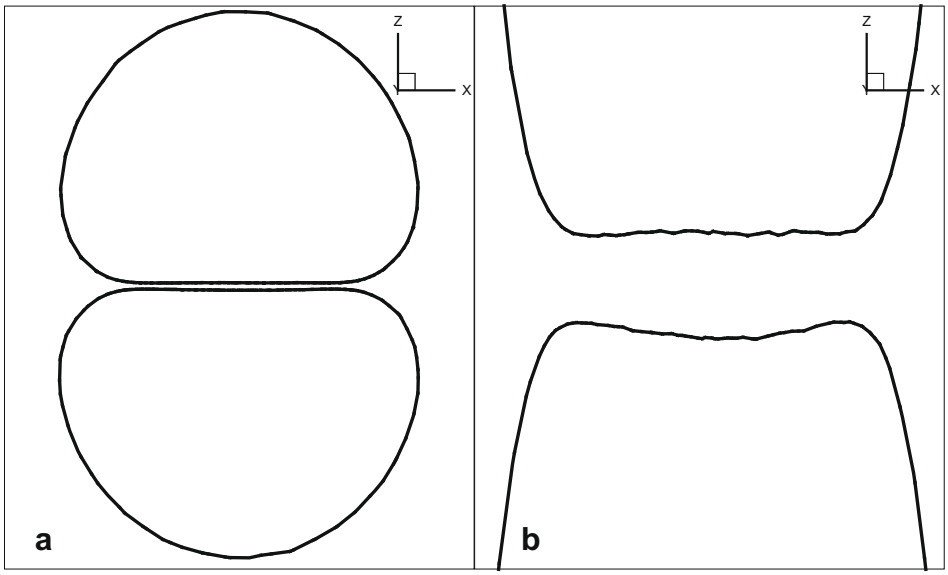

Fig. 7. Details of the gap shape at $t = 0.38$ of the case of Fig. 6. (a) An xz cut through the droplets' centers. (b) An enlarged view of the gap shape with the ratio of x-axis to z-axis distance scaled by 0.1.

observed that the width of the thin film near the center of the film are larger than the width away from the center. This can be clearly seen in the enlarged view of the thin film in Fig. 7(b) where the length ratio between the x-axis and z-axis is scaled by 0.1. A dimple is created on each droplet in the thin film region. Similar film shapes were reported in prior investigations [37,11]. It is noted that the interfaces of the thin film are not smooth; this might be ripples due to instabilities of the interface or numerical errors where the mesh might not be fine enough. A much finer mesh might be needed to address this problem, which will be discussed later.

The history of the minimum gap width (h) is displayed in Fig. 8, where the gap width is non-dimensionalized by D. It is clear the gap width decreases very quickly in the early stage, while it changes very slowly in the late stage. The minimum non-dimensional gap width in our simulation is around 1.5%. The minimum gap width reported in [28] is also around 1.5% for the simulations of near-contact motion of deformable drops using a boundary integral method. The details of the interior mesh when the is gap width is around 1.5% are shown in Fig. 1, and it is clear that mesh quality and mesh resolution are good

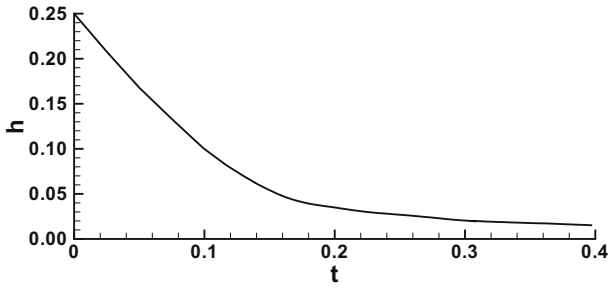

Fig. 8. Evolution of the gap width for the case in Fig. 6.

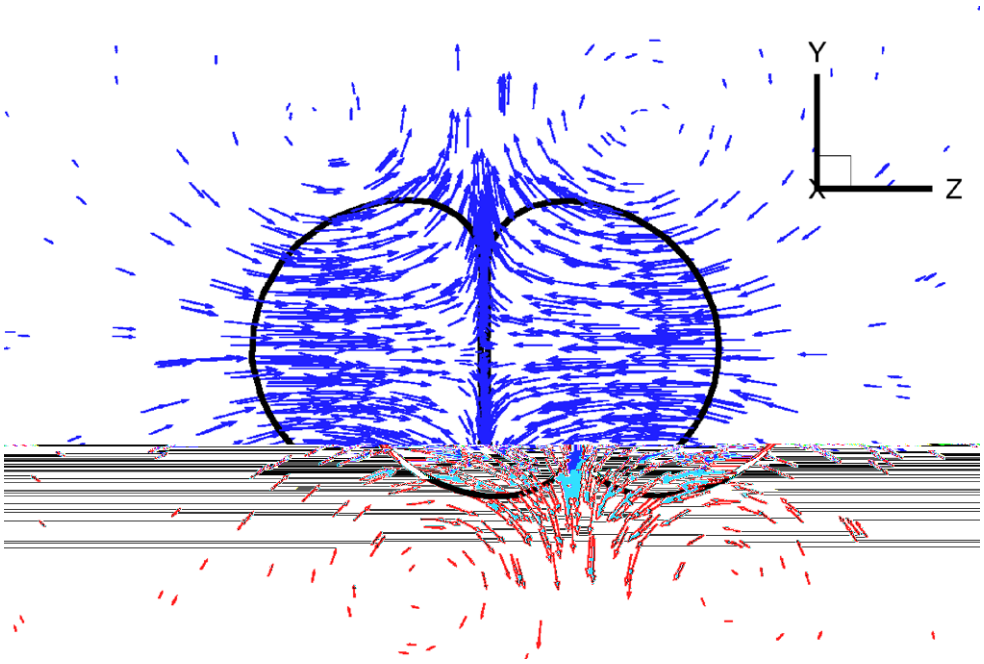

Fig. 9. Velocity field at $t = 0.38$ for the case in Fig. 6.

enough to obtain reasonable results. The velocity field at $t = 0.38$ is shown in Fig. 9. The velocities in the gap almost align with y direction, and two vortex rings are observed.

5.2. Head-on coalescence

To test the capability of the mesh combination scheme, head-on coalescence of a pair of droplets is simulated with $Re = 20.0$ and $We = 0.2$. Initially, the smallest distance between the two droplets is 25% of the droplet diameter. The initial velocity field is obtained using the same method in the previous section. The evolution of the droplet shapes is displayed in Fig. 10. These results show that the droplets are almost undeformed when they are in close proximity (see Fig. 10(b)), because the surface tension forces dominate. It is also should be noted that there are some differences between Fig. 10(b) and (c). Fig. 10(c) shows the shape just after the mesh combination is applied, while Fig. 10(b) displays the shape just before the coalescence. Due to the high curvature in the bridge region and the approaching motion of the two ends of the droplet pair, the radius of the bridge part increases rapidly (Fig. 10(c)–(h)), and then a bulge is created in the center (Fig. 10(i) and (j)). Then, due to the rapid motion of the two ends with large curvatures, a dimpled droplet is formed (Fig. 10(k)). The dimple can be seen clearly in Fig. 10(k′), which is another view of Fig. 10(k). The dimple moves outward, and a prolate spheroid is formed (Fig. 10(l)). Finally, the droplet experiences damped oscillation (Fig. 10(m)–(o)) until the energy is diminished by viscous forces. The interior mesh in yz plane for the droplets' head-on collision is depicted in Fig. 11, and it is clear that the mesh adaptations work well. The details of the mesh including both the interior and the interface elements are shown

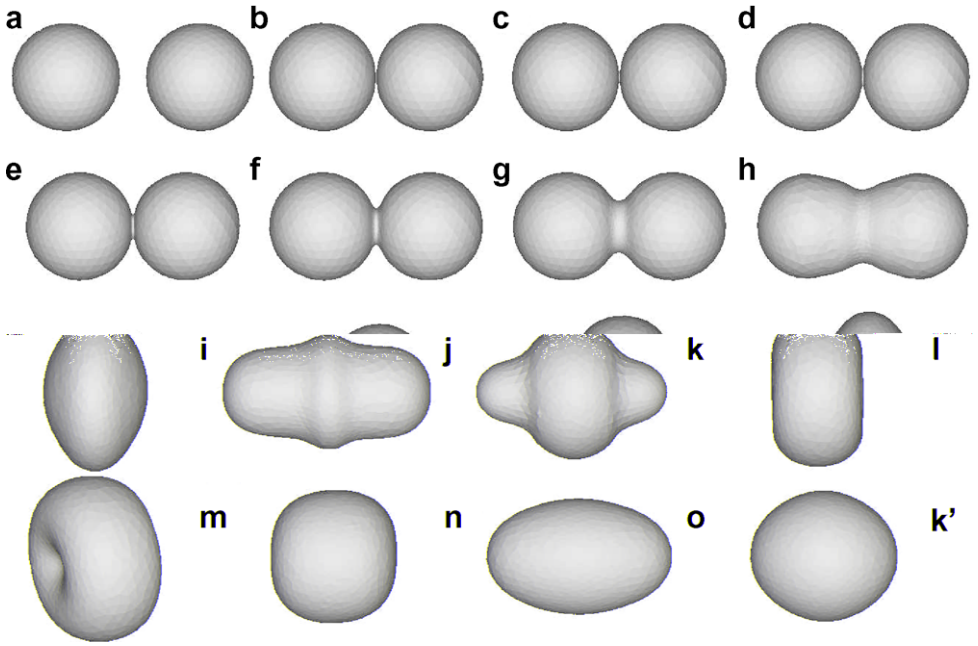

Fig. 10. Snapshots of the droplets head-on collision. $Re = 20.0$ and $We = 0.2$. (k′) is another view of (k) to facilitate a clear observation of the dimple. The non-dimensional time sequence for image (a) to image (o) is 0.0, 0.145, 0.145, 0.147, 0.148, 0.150, 0.155, 0.166, 0.191, 0.233, 0.275, 0.333, 0.363, 0.431, and 0.511.

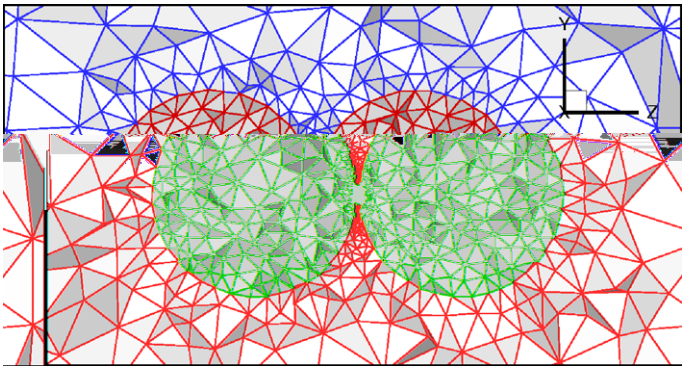

Fig. 11. Interior mesh of the droplets' head-on collision in Fig. 10(c). The mesh for droplets is colored red and shaded dark gray, and the mesh for the suspending phase is colored blue and shaded light gray. (For interpretation of the references in colour in this figure legend, the reader is referred to the web version of this article.)

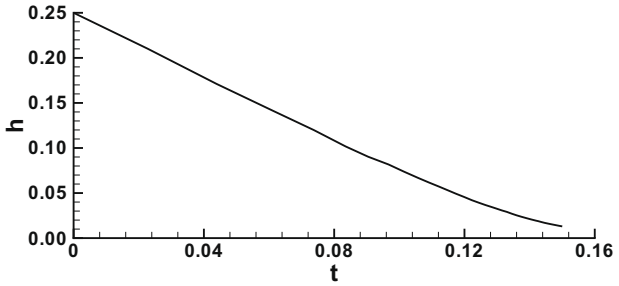

Fig. 12. Evolution of the smallest distance between the two droplets before coalescence of the case in Fig. 10.

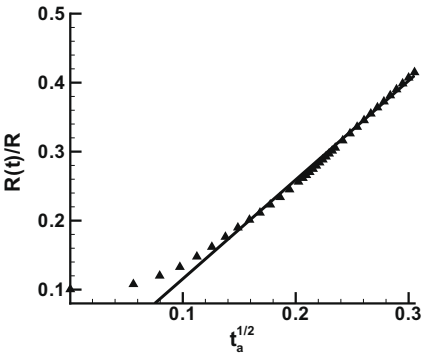

Fig. 13. Evolution of the smallest radius in the bridge region of the case in Fig. 10. The symbol t_a (time after combination) is non-dimensionalized by time $t_i = \sqrt{\rho_d (D/2)^3/\sigma}$. The solid line is a fitted straight line.

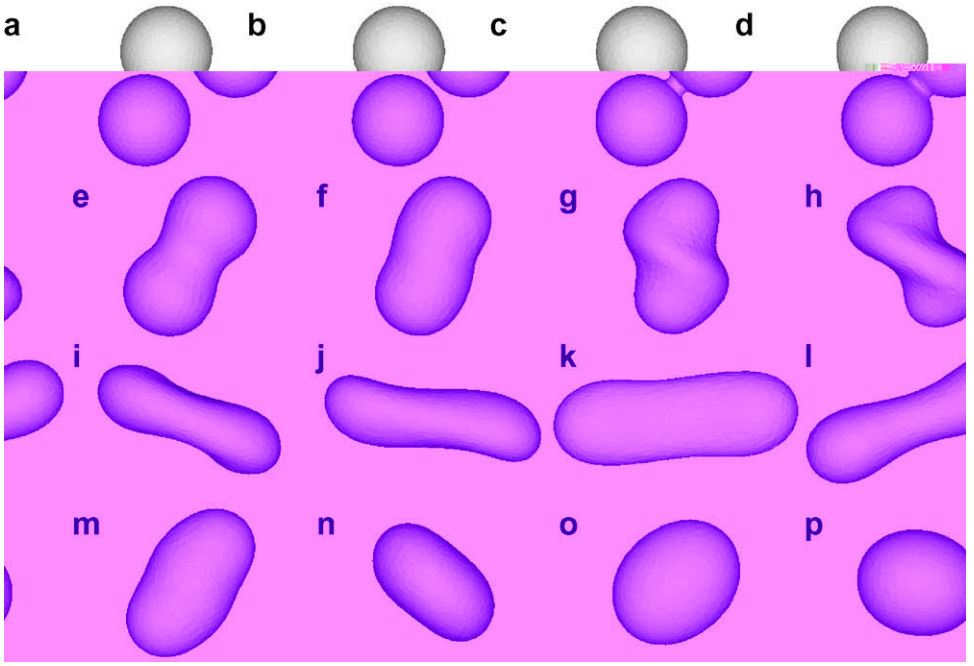

Fig. 14. Snapshots of the droplets off-center collision. $Re = 40.0$ and $We = 0.8$. The non-dimensional time sequence for image (a) to image (p) is 0.0, 0.250, 0.256, 0.291, 0.441, 0.541, 0.631, 0.771, 0.941, 1.101, 1.350, 1.850, 2.650, 3.100, 3.850, and 5.000.

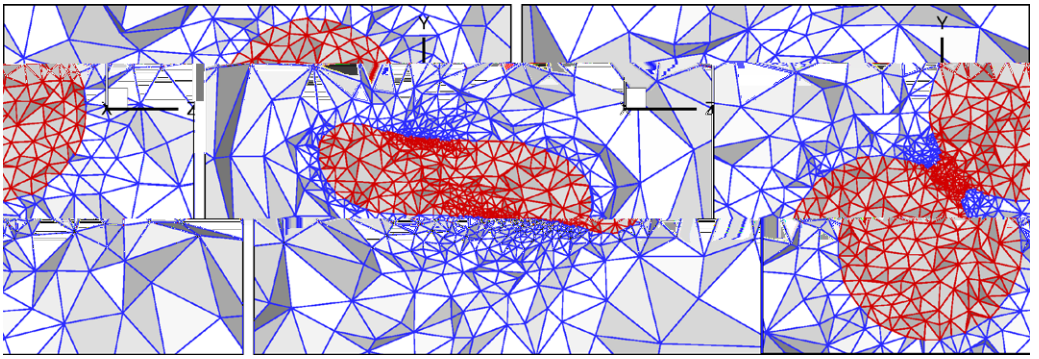

Fig. 15. Interior meshes corresponding to Fig. 14(c) and (j). Mesh is colored and shaded the same way as in Fig. 11. For clarity, the two figures are not in the same scale.

in Fig. 3. The mesh quality and resolution are good enough to obtain reasonable physics and also to achieve computing efficiency. The history of the smallest distance between the two droplets is displayed in Fig. 12. The distance decreases quickly in the early stage but changes slowly in the late stage.

The history of the minimum radius of the bridge that connects the nearest surfaces in droplet coalescences has been investigated by a number of researchers [38–40,9]. The radius evolution of the head-on collision in Fig. 10 is plotted in Fig. 13, where the symbols are the numerical results. A characteristic time t_i is introduced as $t_i = \sqrt{\rho_d (D/2)^3/\sigma}$ [40,9]. We denote the time after combination as t_a, which is non-dimensionalized by t_i. It can be seen that the numerical results align with the fitted straight line, except the data near the origin. The $\sqrt{t_a}$ dependency of the bridge radius (i.e. $R(t)/R \propto \sqrt{t_a}$) was also reported in [38–40,9] for low viscosity fluids. The Reynolds number of the simulation based on the capillary velocity ($Re_c = \rho_d \sigma R/\mu_d$ [9] with R being the radius of the spherical droplets) is 1000, which indicates that the viscous force effect on the evolution of the bridge is minimal. Some reasons for the error are: the outer surface of the bridge region when the mesh combination is applied is assumed to be a surface of rotation of a quadratic curve in our simulations. Further, the time when the mesh combination is applied might be in error.

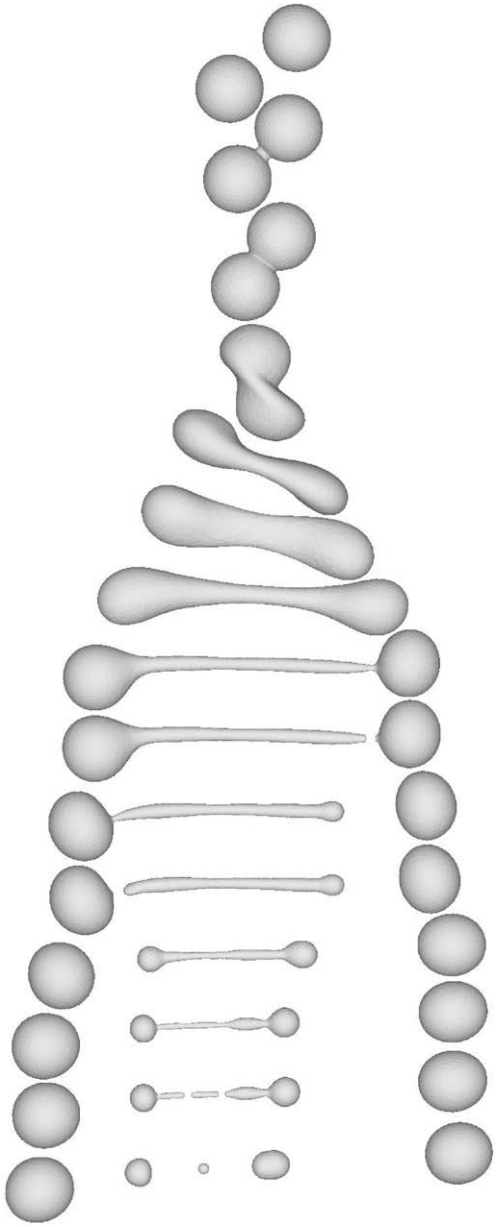

Fig. 16. Snapshots of the droplets off-center collision. $Re = 80.0$ and $We = 32.0$. Time sequence non-dimensionalized by t_c from the top to the bottom is 0.0, 0.511, 0.577, 0.820, 1.322, 1.702, 2.502, 3.718, 3.745, 4.201, 4.241, 4.861, 5.130, 5.139, and 5.463.

5.3. Off-center coalescence

The generality of the mesh combination and mesh separation schemes in dealing with the topological transitions in multiphase flows is tested by simulating off-center coalescences of two droplets. Such oblique collisions are statistically much more likely than head-on collisions. The impact parameter (the non-dimensional perpendicular distance between the axes of motion of the two droplets) is 0.75 for all the simulations reported here. The initial condition is obtained using the same method as the one in the near-contact motion of head-on collision.

Fig. 14 shows the shape evolution of the off-center collision of a pair of droplets with $Re = 40.0$ and $We = 0.8$. After the mesh combination scheme is applied (Fig. 14(c)), a smooth bridge connecting two droplet is created. *It should be noted that for the off-center collision, the shape of the bridge might not be symmetric. However, the exact shape of the bridge is not known a priori. For simplicity, an axisymmetric bridge is used here.* Due to high surface tension forces in this region, the radius increases quickly (Fig. 14(d)–(f)). At the same time, the two ends continue moving in opposite directions due to the momentum, and the droplet is stretched (Fig. 14(g)–(h)). Then, a ligament with two bulbous ends is formed (Fig. 14(i)–(l)). The two ends move toward the center due to the high surface tension forces there. Finally, the droplet becomes a sphere (Fig. 14(p)). It should be noted that the droplet is rotating as it deforms, and it rotates around 225°. The rotation was also observed in Gotaas et al.'s work [13]. The interior meshes at two different stages (Fig. 14(c) and (j)) are displayed in Fig. 15. It is clear that the mesh adaptation schemes are capable of maintaining good mesh quality and mesh resolution.

The second simulation case of the droplet off-center collision is the same as the previous one except that this second case has more initial momentum and a smaller surface tension coefficient. The Reynolds number is 80.0, and Weber number is 32.0.

6. Conclusions and discussion

A mesh combination scheme and a more general mesh separation method are developed to handle the topological changes in multiphase flow simulations using the moving mesh interface tracking method (MMIT). An extra mesh adaptation criterion is also proposed and tested.

Numerous cases of three-dimensional droplets colliding in another viscous fluid are simulated, including head-on and off-center collisions. For the near contact-motion of a pair of droplets, the extra mesh adaptation criterion based on the averaged length of the interior edges is tested, and it is found that the mesh adaptation scheme is capable of capturing the tiny length scales in the region of the drainage, as small as 1.5% of the droplet diameter, and the velocity field near the region is well resolved. The mesh combination scheme is capable to dealing with interface merging, such as droplet coalescence, both head-on and off-center. The results show that the evolution pattern of the smallest radius of the bridge region for the head-on coalescence agrees with the experimental and analytical predictions. Combining the general mesh separation and the mesh combination, an off-center collision of a droplet pair with high Reynolds number and Weber number is simulated, and three satellite droplets are observed in the simulation.

In the present simulations, the time when the mesh separation and/or the mesh combination are/is applied is somewhat ad hoc. The mesh separation is executed when the radius of the neck region is very small (less than 5% of the initial characteristic length), and the mesh combination scheme to permit merging proceeds when the width of the gap between drops is small (around 5% of the diameter of the initial drops). It also should be noted that these two schemes are implemented by converting one fluid to another liquid, so there is always mass gain or mass loss for either phase. The mass gain errors due to the mesh connection for all the simulations are less than 0.4%. For the head-on collision, the mass gain error is as small as 0.045% of the liquid mass. The mass loss errors based on the mass of the initial two spherical droplets due to mesh separation are less than 0.1%. One could minimize the mass gain and mass loss by converting as few elements as possible, i.e. by applying mesh separation for even smaller radius of the thin thread in the separation region, and mesh combination for even tinier gap width of the bridge. However, the computational time will be dramatically increased because many more elements are needed to resolve the smaller length scales. As demonstrated in this work, this method has the potential to investigate detailed physics, such as the physics of the drainage and the initial coalescence. A promising future approach to modeling the challenge multiphase flows would be to couple this method with some theoretical analysis which could help to determine the time when coalescence or breakup occurs as well as the shape of the bridge.

References

[1] S.P. Quan, D.P. Schmidt, A moving mesh interface tracking method for 3D incompressible two-phase flows, J. Comput. Phys. 221 (2007) 761–780.
[2] J.M. Rallison, The deformation of small viscous drops and bubbles in shear flows, Ann. Rev. Fluid Mech. 16 (1984) 45–66.
[3] H.A. Stone, B.J. Bentley, L.G. Leal, An experimental study of transient effects in the breakup of viscous drops, J. Fluid Mech. 173 (1986) 131–158.
[4] J.C. Burton, R. Waldrep, P. Taborek, Scaling and instabilities in bubble pinch-off, Phys. Rev. Lett. 94 (18) (2005) 184502.
[5] N. Ashgriz, J. Y Poo, Coalescence and separation in binary collisions of liquid-drops, J. Fluid Mech. 221 (1990) 183–204.
[6] J. Qian, C.K. Law, Regimes of coalescence and separation in droplet collision, J. Fluid Mech. 331 (1997) 59–80.
[7] S. Guido, M. Simeone, Binary collision of drops in simple shear flow by computer-assisted video optical microscopy, J. Fluid Mech. 357 (1998) 1–20.
[8] H. Yang, C.C. Park, Y.T. Hu, L.G. Leal, The coalescence of two equal-sized drops in a two-dimensional linear flow, Phys. Fluids 13 (2001) 1087–1106.
[9] D.G.A.L. Aarts, H.N.W. Lekkerkerker, H. Guo, G.H. Wegdam, D. Bonn, Hydrodynamics of droplet coalescence, Phys. Rev. Lett. 95 (2005) 164503.
[10] F. Baldessari, L.G. Leal, Effect of overall drop deformation on flow-induced coalescence at low capillary numbers, Phys. Fluids 18 (2006) 013602.
[11] Y. Yoon, F. Baldessari, H.D. Ceniceros, L.G. Leal, Coalescence of two equal-sized deformable drops in an axisymmetric flow, Phys. Fluids 19 (2007) 102102.
[12] B. Lafaurie, C. Nardone, R. Scardovelli, S. Zaleski, G. Zanetti, Modelling merging and fragmentation in multiphase flows with SURFER, J. Comput. Phys. 113 (1994) 134–147.
[13] C. Gotaas, P. Havelka, H.A. Jakobsen, H.F. Svendsen, M. Hase, N. Roth, B. Weigand, Effect of viscosity on droplet–droplet collision outcome: experimental study and numerical comparison, Phys. Fluids 19 (2007) 102106.
[14] M. Sussman, P. Smereka, S. Osher, A level set approach for computing solutions to incompressible 2-phase flow, J. Comput. Phys. 114 (1994) 146–159.
[15] Y. Pan, K. Suga, Numerical simulation of binary liquid droplet collision, Phys. Fluids 17 (2005) 082105.
[16] S. Tanguy, A. Berlemont, Application of a level set method for simulation of droplet collisions, Int. J. Multiphase Flow 31 (2005) 1015–1035.
[17] T. Inamuro, T. Ogata, S. Tajima, N. Konishi, A lattice Boltzmann method for incompressible two-phase flows with large density differences, J. Comput. Phys. 198 (2004) 628–644.
[18] M.R. Nobari, Y.J. Jan, G. Tryggvason, Head-on collision of drops – a numerical investigation, Phys. Fluids 8 (1996) 29–42.
[19] M.R.H. Nobari, G. Tryggvason, Numerical simulations of three-dimensional drop collisions, AIAA J. 34 (1996) 750–755.
[20] D.J. Torres, J.U. Brackbill, The point-set method: front-tracking without connectivity, J. Comput. Phys. 165 (2000) 620–644.
[21] S. Shin, D. Juric, Modeling three-dimensional multiphase flow using a level contour reconstruction method for front tracking without connectivity, J. Comput. Phys. 180 (2002) 427–470.
[22] R.J. Leveque, Z. Li, The immersed interface method for elliptic equations with discontinuous coefficients and singular sources, SIAM J. Numer. Anal. 31 (1994) 1019–1044.
[23] L. Lee, R.J. Leveque, An immersed interface method for incompressible Navier–Stokes equations, SIAM J. Sci. Comput. 25 (2003) 832–856.
[24] R.P. Fedkiw, T. Aslam, B. Merriman, S. Osher, A non-oscillatory Eulerian approach to interfaces in multimaterial flows (the Ghost fluid method), J. Comput. Phys. 152 (1999) 457–492.
[25] M. Kang, R. Fedkiw, X.-D. Liu, A boundary condition capturing method for multiphase incompressible flow, J. Sci. Comput. 15 (2000) 323–360.
[26] M. Sussman, K.M. Smith, M.Y. Hussaini, R. Ohta, R. Zhi-Wei, A sharp interface method for incompressible two-phase flows, J. Comput. Phys. 221 (2007) 469–505.
[27] R.R. Nourgaliev, M.S. Liou, T.G. Theofanous, Numerical prediction of interfacial instabilities: sharp interface method (SIM), J. Comput. Phys. 227 (2008) 3940–3970.
[28] V. Cristini, J. Blawzdziewicz, M. Loewenberg, An adaptive mesh algorithm for evolving surfaces: simulations of drop breakup and coalescence, J. Comput. Phys. 168 (2001) 445–463.
[29] A. Anderson, X.M. Zheng, V. Cristini, Adaptive unstructured volume remeshing I: the method, J. Comput. Phys. 208 (2005) 616–625.

[30] X.M. Zheng, J. Lowengrub, A. Anderson, V. Cristini, Adaptive unstructured volume remeshing - II: application to two- and three-dimensional level-set simulations of multiphase flow, J. Comput. Phys. 208 (2005) 626–650.
[31] M.Z. Dai, D.P. Schmidt, Numerical simulation of head-on droplet collision: Effect of viscosity on maximum deformation, Phys. Fluids 17 (2005) 041701.
[32] S.P. Quan, D.P. Schmidt, Direct numerical study of a liquid droplet impulsively accelerated by gaseous flow, Phys. Fluids 18 (2006) 102103.
[33] M.Z. Dai, D.P. Schmidt, Adaptive tetrahedral meshing in free-surface flow, J. Comput. Phys. 208 (2005) 228–252.
[34] B. Perot, R. Nallapati, A moving unstructured staggered mesh method for the simulation of incompressible free-surface flows, J. Comput. Phys. 184 (2003) 192–214.
[35] X.D. Liu, R.P. Fedkiw, M.J. Kang, A boundary condition capturing method for Poisson's equation on irregular domains, J. Comput. Phys. 160 (2000) 151–178.
[36] W. Chang, F. Giraldo, B. Perot, Analysis of an exact fractional step method, J. Comput. Phys. 180 (2002) 183–199.
[37] S. Abid, A.K. Chesters, The drainage and rupture of partially-mobile films between colliding drops at constant approach velocity, Int. J. Multiphase Flow 20 (1994) 613–629.
[38] J. Eggers, J.R. Lister, H.A. Stone, Coalescence of liquid drops, J. Fluid Mech. 401 (1999) 293–310.
[39] L. Duchemin, J. Eggers, C. Josserand, Inviscid coalescence of drops, J. Fluid Mech. 487 (2003) 167–178.
[40] M.M. Wu, T. Cubaud, C.M. Ho, Scaling law in liquid drop coalescence driven by surface tension, Phys. Fluids 16 (2004) L51–L54.